Soft Matter

RSC Publishing

PAPER

View Article Online
View Journal | View Issue

Cite this: *Soft Matter*, 2013, **9**, 2458

Improved pH-responsive amphiphilic carboxymethyl-hexanoyl chitosan–poly(acrylic acid) macromolecules for biomedical applications†

Meng-Hsuan Hsiao, Kuan-Hui Lin and Dean-Mo Liu*

Received 12th November 2012
Accepted 13th December 2012

DOI: 10.1039/c2sm27610k

www.rsc.org/softmatter

In this communication, we report a new type of amphiphilic carboxymethyl-hexanoyl chitosan (CHC)–poly(acrylic acid) (PAA) hybrid macromolecule, which was successfully prepared through polymerization of acrylic acid (AA) in the presence of amphiphilic CHC. The chemical structure of the hybrid was characterized by FT-IR and ^{1}H NMR, which confirmed a chemical linkage between the amine groups of CHC and hydroxyl groups of AA. This CHC–PAA hybrid exhibited amphiphilic property as the original CHC rendering the self-assembling capability to be tunable in terms of AA concentration. Compared with the existing pristine chitosan–PAA co-polymers, this CHC–PAA hybrid exhibited a relatively high pH-responsive volumetric change by 10–100 times compared with the existing alternatives reported in the literature. The hybrid nanoparticles showed excellent encapsulation efficiency greater than 90% for a hydrophobic anti-cancer substance, (*S*)-(+)-camptothecin. A pH-responsive drug release behavior was systematically evaluated. Besides, this hybrid also revealed excellent cytocompatibility towards the MCF-7 and BCE cell lines, which, associated with its structural stability, suggests this new type of CHC–PAA hybrid to be a promising biomaterial for oral drug delivery application.

1 Introduction

Polymer micelles or nanoparticles have been widely investigated as drug carriers for anticancer therapy,[1–3] they have been frequently utilized due to their beneficial properties such as specific functionality, stabilized nanostructures, high drug loading capacity, biodegradability and low toxicity. Therefore, to meet the requirement of targeting tumor tissues, stimuli responsive nanocarriers emerged as novel controlled drug release systems operated by appropriate stimuli, such as temperature, light, mechanical forces, pH and enzymes. A pH-sensitive polymeric nanocarrier would be more useful for targeting tumor tissues because these sites are more acidic than other normal tissues, such as endosomes (pH 5–6) and lysosomes (pH 4–5).[4–7] A vast number of natural and synthetic polymers have been used to prepare nanocarriers for cancer therapy.[8–27] Among them, chitosan (CS) is particularly attractive owing to its biological activity, low toxicity, biocompatibility and biodegradability. Self-aggregated nanoparticles or micelles based on amphiphilic chitosan derivatives, such as glycol chitosan carrying 5β-cholanic acid,[14] glycidol-chitosan-deoxycholic acid,[15] hydrotropic oligomer-conjugated glycol chitosan[16] and 6-mercaptopurine-carboxymethyl chitosan,[17] have been extensively reported for applications in, for instance, delivering conventional drugs,[15] peptides,[14] and DNA[18] for cancer therapy. One important advantage of those pH-sensitive polymer nanocarriers is that they can be designed responsive to acidic endosomal pH, which can accelerate drug release in acidic endosomes and even release drugs into the cytosol. This will surely be more critical for those anti-cancer drugs suffering from multidrug resistant (MDR) capability of specific tumor cells, due to increased efflux activity, which was induced through over expressing ATP binding cassette (ABC) proteins.[24–35]

Therefore, it is more interesting to enhance the pH sensitivity of either pristine or modified chitosan to render drug release behavior subjected to higher pH responsiveness. This will be more medicinally useful if the chitosan-based nanocarriers can be adapted for oral application. In other words, it requires a minimal leakage at an acidic environment, *i.e.*, stomach, but enhances drug release to a certain extent under more alkaline environment, *i.e.*, GI track. Therefore, to boost pH responsive behavior of the chitosan, acrylic acid (AA) has been employed. However, numerous reports addressed a small pH-induced volume change, by 1–10 times or only fractions, giving rise to a less pH responsiveness.[28–30] However, since the different response of amine groups or hydroxyl or particularly carboxyl groups (in many modified chitosan-based derivatives) of the modified chitosan with respect to a change in environmental pH was observed, a net responsiveness toward a change

Department of Materials Sciences and Engineering, National Chiao Tung University, 1001 Ta-Hsueh Rd, Hsinchu, 300 Taiwan. E-mail: deanmo_liu@yahoo.ca; Fax: +886 3 572 4727; Tel: +886 3 571 2121 ext. 55391

† Electronic supplementary information (ESI) available. See DOI: 10.1039/c2sm27610k

in pH may be reduced to a certain extent, as a consequence, weakening the potential therapeutic efficacy. Therefore, it is an alternative and new approach to employ an amphiphilic chitosan (termed as CHC), which was successfully prepared and reported from this lab,[31,32] to form a hybrid molecule with the incorporation of AA. Following a previous work on the synthesis of this amphiphilic CHC,[33] a further chemical modification along the CHC molecule, as a starting template, was performed using acrylic acid. We do expect the chemical modification by AA being able to react with more amine groups by radical reaction and making the resulting hybrid more responsive to pH change. In this study, we successfully synthesized a new CHC–PAA hybrid macromolecule where the chemical structure, colloidal properties, cytocompatibility, and pH-responsive drug release behavior of the hybrid were systematically investigated.

2 Experimental

2.1 Materials

Carboxymethyl-hexanoyl chitosan (CHC), a self-assembled nanoparticle, was bought from Advance Delivery Technology Inc., Hsinchu, Taiwan. Acrylic acid (AA), ammonium persulfate (APS), (*S*)-(+)-camptothecin (95%, CPT), dimethyl sulfoxide (DMSO), pyrene, ninhydrin reagent, fetal bovine serum, and dialysis tubing cellulose membrane (M_w cut-off 12 400 g mol^{-1}, avg. flat width 33 mm) were purchased from Sigma-Aldrich. Phosphate buffered saline (PBS) was purchased from UniRegion Bio-tech, Taiwan. Chitosan (M_w = 210 000, degrees of deacetylation = 91.3%) was bought from C&B company, Taiwan.

2.2 Synthesis of pH-sensitive CHC–PAA hybrid macromolecules

According to previous studies, the amphiphilic chitosan was successfully synthesized through carboxymethyl and hydrophobic hexanoyl substitutions,[33] the as-received amphiphilic chitosan was chemically modified with acrylic acid. 0.1 g of CHC was first dissolved and dispersed in 50 ml of DI water under vigorous agitation at room temperature for 24 hours until the CHC was fully dissolved. Sequentially, 35, 75 and 140 μl of AA monomers were added to 50 ml CHC solution with stirring for 2 hours and then added 0.02 g of radical initiator (APS), the solution was purged with nitrogen and heated to 70 °C in an oil bath. After 2 hours of reaction, the resulting solution was collected using a dialysis membrane with pH 9 buffer solution for 72 hours to remove the residual APS and unreacted monomers. The dialysis dispersion solution was frozen at −20 °C for 24 hours, and then lyophilized to obtain CHC–PAA. The reaction conditions and sample numbers are listed in Table 1. The molar ratios of CHC and AA are based on the moles of the amide unit in CHC to the moles of acrylic acid.

2.3 Preparation of self-assembled CHC–PAA nanoparticles

The CHC–PAA powder was suspended in distilled water under gentle shaking at 25 °C for a few minutes until well dissolved, followed by ultrasonication using a probe sonifier (Automatic Ultrasonic Processor UH-500A, China) at 30 W for 1 minute. To inhibit the heat buildup during sonication, the pulse function was used (pulse on 5.0 s: pulse off 1.0 s).

Table 1 Reaction conditions, sample names, and degree of substitution (DS) of CHC–PAA hybrids and estimation of amine yield of CHC and CHC–PAA by ninhydrin. (n = 3)

Sample no.	M[a] (mol L^{-1})	NH_2 : AA[b]	DS%	CHC[c] (%)
CHC	2.12 ± 0.02	—	—	100
CHCA1	1.12 ± 0.06	1 : 1	47.2 ± 2.7	52.7 ± 2.8
CHCA3	0.89 ± 0.05	1 : 3	58.0 ± 2.3	42.1 ± 2.4
CHCA6	0.74 ± 0.01	1 : 6	65.1 ± 0.6	34.8 ± 0.5

[a] M is the molar concentration of the amine group in 0.1% CHC or CHC–PAA solutions. [b] NH_2 means the NH_2 amount of CHC hybrids measured by a ninhydrin test. [c] CHC (%) means the concentration of amine on CHC or CHC–PAA hybrids, the amine concentration of starting CHC was considered to be 100%.

2.4 Characterization

Fourier transform infrared (FT-IR) spectroscopy and nuclear magnetic resonance (NMR) were used for identifying the molecular structure of the CHC–PAA hybrid macromolecule. The FT-IR spectra of KBr pellets were recorded (32 scans with resolution of 4 cm^{-1}) on a Unican Mattson Mod 7000 FTIR spectrophotometer. ^{1}H NMR spectra were recorded at 300 MHz on a (7.05 T) BRUKER DRX-300 NMR spectrometer. The substitution degree of CHC–PAA hybrid macromolecules was measured by a ninhydrin test. The method can directly detect the free amine group on the glucosamine repeat unit of chitosan.[34,35] The ninhydrin reagent (2 ml, Sigma) was added to 1 ml of 0.1% (w/w) CHC–PAA solutions and the tubes were placed in the boiling water bath for 30 min. The suspension of the tubes was subjected to centrifugation at 3000 rpm for 10 min, then, the UV-vis absorption of supernatants of the tubes was monitored at 570 nm using a UV-visible spectrometer (Evolution 300, Thermo). The structural morphology of the CHC–PAA nanoparticles was observed using a Transmission Electron Microscope (TEM) (JEOL2100, Japan). The mean size and zeta potential of the CHC–PAA nanoparticles were monitored by dynamic light scattering (Delsa™ Nano C, Beckman).

2.5 Self-assembly behavior of CHC–PAA hybrid macromolecules

The critical aggregation concentration (CAC) of CHC–PAA hybrids was measured with pyrene, a common fluorescence probe used to monitor the self-aggregation behavior of surfactants and polymers. A fluorescence spectrophotometer (Hitachi FL-4500, Japan) was used for obtaining the emission spectra of pyrene. A number of CHC–PAA solutions containing 1–2 μM of pyrene were excited at 343 nm, and the fluorescence emission spectra were recorded in the 350–500 nm wavelength range.

2.6 Drug loading and release

The drug release behavior of CHC–PAA nanoparticles was evaluated by using (*S*)-(+)-camptothecin (CPT), a hydrophobic anti-cancer drug, as the model molecule. CHC–PAA

nanoparticles containing CPT drug was prepared by the following processes. Concisely, CPT was simply dissolved in DMSO to prepare 1 mg ml^{-1} of CPT–DMSO solution, and then, well mixed with distilled water (0.5/9.5 v/v) until a homogeneous appearance was visually observed. The CPT concentration of the final solution is 50 μg ml^{-1}. 1 mg of the as-prepared CHC–PAA powder was added into 1 ml of the drug solution and stirred at room temperature for 1 day. The drug-containing nanoparticles were separated from the aqueous phase by centrifugation at 12 000 rpm and 20 °C for 15 min. The drug concentration of the supernatant was analyzed by the ultraviolet absorption (UV) at a wavelength of 366 nm, a specific absorption band of CPT, with reference to a calibration curve on a UV-visible spectrometer (Evolution 300, Thermo scientific) in triplicate. The drug encapsulation efficiency (EE) can be calculated by the following equation:

$$\text{Drug encapsulation efficiency} = (I_{\text{total}} - I_{\text{remaining}})/I_{\text{total}} \times 100\%$$

where I_{total} is the UV absorption intensity of free CPT, $I_{\text{remaining}}$ is the UV absorption intensity of CPT remaining in the supernatant.

1 mg ml^{-1} of CPT–DMSO solution was added into PBS buffers with different pH values from 4.5 to 7.5, individually, to prepare 50 μg ml^{-1} drug solutions. And then, CHC–PAA powder was dissolved in the drug solutions with different pH values at 25 °C, and the entire system was kept at 37 °C with continuous magnetic stirring. At a predetermined time point, the test tubes were subjected to centrifugation at 12 000 rpm for separating the supernatant and suspension from the release medium. The supernatant was used to estimate the concentration of drug *via* UV-vis spectroscopy. The precipitation at the bottom of the test tubes was refilled with a fresh PBS medium and repeated the procedure of the centrifugation and UV analysis over a predetermined period of time to monitor the release kinetics of CPT. Each data were measured in triplicate.

2.7 Cell cytotoxicity

The human breast adenocarcinoma cell (MCF-7) and bovine corneal endothelial cell (BCE) were maintained in separated cultivating medium with DMEM (Dulbecco's modified Eagle's medium) supplemented with 1% penicillin/streptomycin and 10% fetal bovine serum (FBS) at 37 °C in a humidified atmosphere of 5% CO_2 in air. *In vitro* cytotoxicity of the CHC–PAA nanoparticles with different AA/CHC ratios was examined using MCF-7 and BCE cell lines. Briefly, 1×10^4 cells were transferred to a 96-well plate to allow the cells to attach and expose to a serial concentration of the CHC–PAA nanoparticles. After incubation for 1 or 2 days, MTT reagents were added to the wells and incubated for 4 hours, and then the solution was removed and 100 μl of DMSO was added to the wells to dissolve the crystal. The absorbance of the DMSO solution was observed by using a microplate reader at dual wavelength of 570 and 650 nm. Cell viability was determined by the following equation:

$$\text{Cell viability (\%)} = (A_{\text{sample}}/A_{\text{control}}) \times 100\%$$

where A_{sample} and A_{control} represent the absorption intensity of cells treated with different samples and control group (non-treated was set to 100%), respectively.

3 Result

3.1 Synthesis and molecular structure analysis of CHC–PAA hybrid macromolecules

CHC–PAA hybrid macromolecules were prepared by polymerization of acrylic acid monomers grafted on CHC, as shown in Fig. 1. At first, different amounts of acrylic acid were added to CHC solution, and then a radical initiator, ammonium persulfate (APS), was added to the mixed solutions (different molecular ratios of (NH_2 of CHC) : (acrylic acid (AA)) = 1 : 1 (CHCA1), 1 : 3 (CHCA3) and 1 : 6 (CHCA6)). Under the reaction protocol, positively charged CHC was expected to attract more AA molecules in acidic solution, which may permit a preferential radical reaction in the presence of APS between the protonated amine and AA.[36–38] The hydrogen of the amine group on CHC was removed to form a macroradical. The macroradicals can react with the double bond of AA monomers and act as the active site to initiate chain propagation of the monomers.[39] Although the interaction between hydroxyl groups in CHC and AA may occur, it is believed that the reaction yield is negligibly small. Therefore, in forthcoming analysis, we presumed that AA substitution was mainly associated with amine groups in the CHC. After 2 hours of reaction, the resulting solution was purified using a dialysis membrane with DI water for 72 hours to remove the residual APS, PAA homopolymer and unreacted monomers. The dialysis dispersion solution was frozen at −20 °C for 24 hours, and then lyophilized to obtain CHC–PAA hybrids. The molecular structures of CHC–PAA hybrids were then analyzed by FT-IR and NMR.

The chemical structures of pure CHC, PAA and CHC–PAA hybrids were characterized by FT-IR as illustrated in Fig. 2 and Table 2. Fig. 2(a) shows the characteristic absorption peaks of CHC and PAA, wherein the peaks at 1464 cm^{-1} and 1725 cm^{-1} are related to bending mode of $-CH_2-$ of PAA and the presence of C=O stretching mode in the carboxylic acid group of PAA. The characteristic peaks of pure CHC are amide I, amide II and amide III at 1647 cm^{-1}, 1560 cm^{-1} and 1384 cm^{-1}, respectively. In 2004, Fu *et al.* reported that regions of urea group vibrations, the so-called amide I and amide II, were highly complex vibrations: the amide I mode (1800–1600 cm^{-1}) involved the contributions of the C=O stretching, the C–N stretching and the C–C–N deformation.[40] The amide II mode (1600–1500 cm^{-1}) is a mixed contribution of the in-plane N–H bending, C–N stretching and C–C stretching vibrations. After the polymerization reaction, these characteristic absorption peaks became weaker or being masked with other absorption bands, implying that the reactive functional groups of CHC, such as $-NH_2$, have reacted with AA and lost their characteristic peaks in the FTIR spectrum. As expected, the absorption peak of hydroxyl groups remained relatively unchanged in position and intensity, suggesting that the hydroxyl groups in the starting CHC template may be unreacted or in a relatively small yield over the reaction protocol designed in this work. The absorption peaks in the

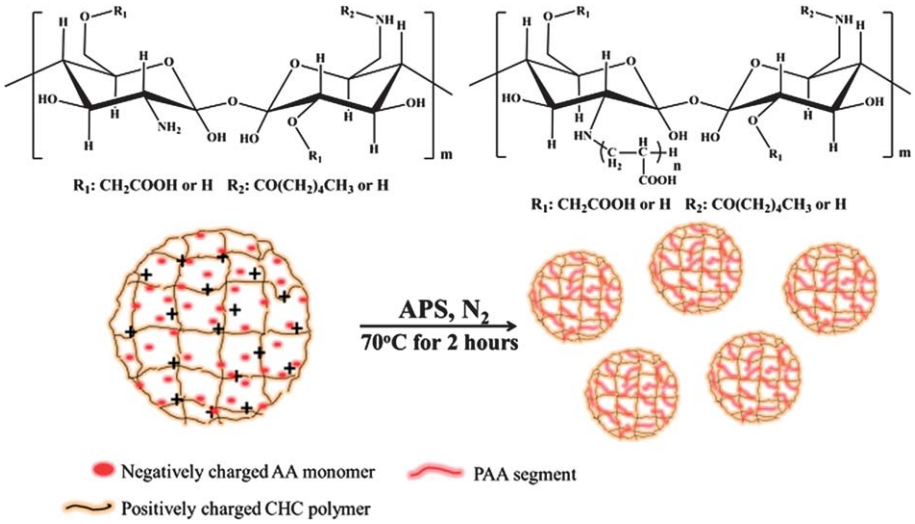

Fig. 1 Preparation of CHC–PAA hybrid macromolecules.

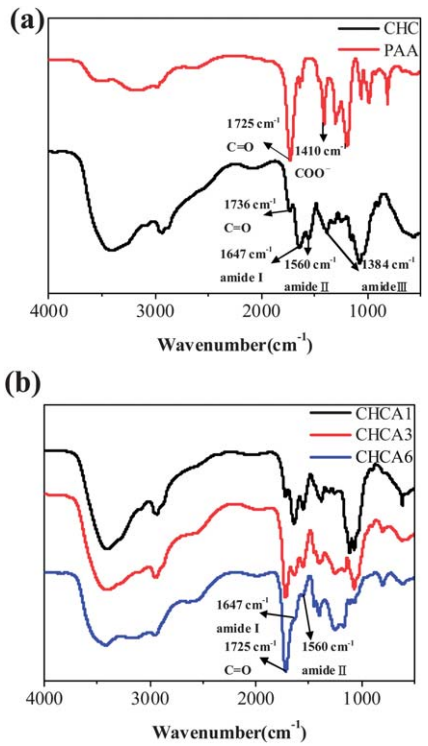

Fig. 2 (a) FT-IR spectra of CHC and PAA. (b) FT-IR spectra of CHCA1, CHCA3 and CHCA6.

spectra of CHC–PAA hybrids are listed in Table 2. It showed that the characteristic peaks of CHC–PAA were C═O stretching vibration (1725 cm^{-1}), amide I (1645 cm^{-1}), amide II (1565 cm^{-1}), $–CH_2–$ bending vibration (1455 cm^{-1}) and $–COO^-$ symmetric stretching (1409 cm^{-1}). The absorbance intensity of the peaks (1725 cm^{-1}, 1455 cm^{-1} and 1409 cm^{-1}) is dependent on the amount of acrylic acid added to CHC solution, which means that more AA was grafted on CHC and polymerization of AA occurred at a higher concentration of acrylic acid.

Table 2 Characteristic peaks of PAA, CHC and CHC–PAA hybrids

Sample	Characteristic absorption peaks
PAA	1725 cm^{-1} (C═O stretching vibration)
	1464 cm^{-1} ($–CH_2–$ scissor vibration)
	1409 cm^{-1} ($–COO^-$ symmetric stretching)
CHC	1736 cm^{-1} (C═O stretching vibration)
	1647 cm^{-1} (amide I), 1560 cm^{-1} (amide II)
	1384 cm^{-1} (amide III)
CHCA1	1725 cm^{-1} (C═O stretching vibration)
	1645 cm^{-1} (amide I), 1565 cm^{-1} (amide II)
	1455 cm^{-1} ($–CH_2–$ scissor vibration)
	1409 cm^{-1} ($–COO^-$ symmetric stretching)
CHCA3	1725 cm^{-1} (C═O stretching vibration)
	1645 cm^{-1} (amide I), 1565 cm^{-1} (amide II)
	1455 cm^{-1} ($–CH_2–$ scissor vibration)
	1409 cm^{-1} ($–COO^-$ symmetric stretching)
CHCA6	1725 cm^{-1} (C═O stretching vibration)
	1645 cm^{-1} (amide I), 1565 cm^{-1} (amide II)
	1455 cm^{-1} ($–CH_2–$ scissor vibration)
	1409 cm^{-1} ($–COO^-$ symmetric stretching)

Furthermore, comparing the peaks of CHC and CHC–PAA, there were significant shifts in characteristic peaks: C═O stretching vibration (from 1736 cm^{-1} to 1725 cm^{-1}), amide I (from 1674 cm^{-1} to 1645 cm^{-1}), and amide II (from 1560 cm^{-1} to 1565 cm^{-1}), supporting PAA grafting on the backbone of CHC.

The chemical structures of CHC and CHC–PAA hybrids, characterized by ^1H NMR, are illustrated in Fig. 3. It shows the absorption spectra of pure CHC that the inherent peaks of CHC such as methyl ($–CH_3–$), methylene ($–CH_2–$) and tertiary carbon hydrogen (–CH–) of the hexanoyl group clearly appear in the spectra at 0.771 ($–CH_3$), 1.076 ($–CH_2–$), 1.199 ($–CH_2–CH_2–$), 1.499 (–CH–) and 2.199 ($–CO–CH_2–$) ppm, respectively. D-solvent (deuterium oxide) has a strong peak at 4.8 ppm. In contrast, the spectra of the CHC–PAA show typical peaks such as methylene ($–CH_2–$) and tertiary carbon hydrogen (–CH–) of PAA in the backbone of CHC–PAA hybrid macromolecules (Fig. 3(b)),

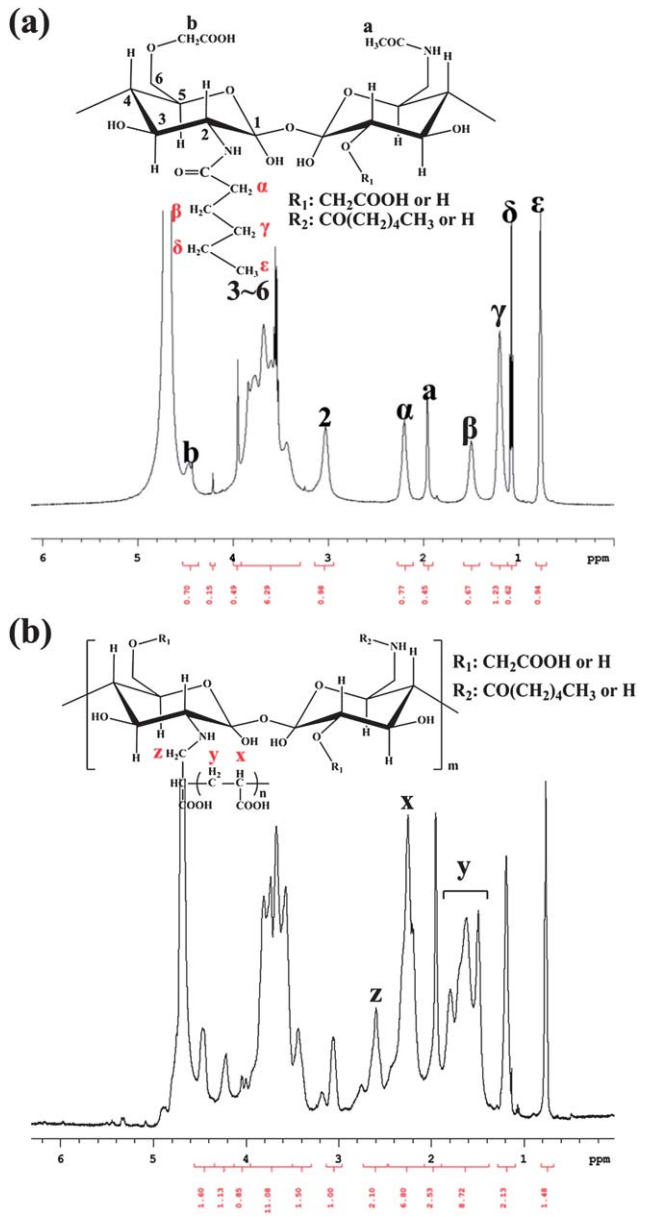

Fig. 3 ^{1}H NMR spectra of (a) CHC and (b) CHC–PAA hybrid macromolecules.

which are clearly exhibited at 1.492–1.953, 2.252–2.753 ppm, respectively. Therefore, it supports that the PAA segments were chemically bonded along the CHC chain.

3.2 Ninhydrin assay

Ninhydrin (triketohydrinedene hydrate) test is a common analysis method for determining the amount of the free amine group of glucosamine units. In this study, the CHC–PAA hybrid was prepared by grafting acrylic acids on amine groups of CHC. Therefore, the degree of substitution (DS) for PAA grafted on the amine group of CHC was quantitatively analyzed by a ninhydrin test, as shown in Fig. 4. The as-received CHC contained 56.23% amine groups (compared with starting amine content in pristine chitosan), in good agreement with data ~52% from the provider, which means that the remaining amine groups of

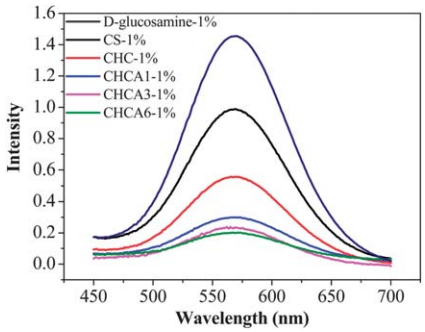

Fig. 4 FTIR spectra of the amine yield of CHC and CHC–PAA.

CHC can be used to graft the AA. The synthesis of CHC–PAA hybrids (CHCA1, CHCA3, and CHCA6) further consumed the amine group of CHC and Table 1 shows the degree of substitution (DS) for AA grafting onto CHC and molar concentration of the remaining amine group of each sample. To normalize the evaluation, the amine groups of starting CHC were set as the default value of 100% and DS was calculated for each sample, where the remaining amine groups on CHC reacted with different amounts of AA to form CHCA1 (with DS = 47.2 ± 2.7%), CHCA3 (DS = 58.0 ± 2.3%), and CHCA6 (DS = 65.1 ± 0.6%). The results indicated that more starting AA consumed more amounts of the remaining amine groups of CHC, leaving a relatively small amount, from 52.7 ± 2.8% (CHCA1), 42.1 ± 2.4% (CHCA2), to 34.8 ± 0.5% (CHCA6), of the amine in the final CHC–PAA hybrids. However, only a part of the amine groups in CHC has been replaced, and in the meantime, part of the hydroxyl groups should also be replaced, for compositions with higher AA concentration, *i.e.*, CHCA3 and CHCA6. The unreacted AA further polymerized to form branched PAA along the CHC, which should contribute to pH sensitivity of the resulting CHC–PAA hybrids. Since the hydrophobic segments, *i.e.*, hexanoyl groups, remained intact on the resulting CHC–PAA hybrid, the self-assembling capability of the newly formed hybrid was expected to remain active.

3.3 Self-assembly behavior

To evaluate the self-assembling ability of the CHC-PAA hybrid in water, pyrene was employed as a fluorescence probe to investigate the self-assembly behavior of the CHC–PAA at a molecular level. Pyrene has been frequently chosen as a fluorescence probe to monitor the self-assembly behavior of amphiphilic polymers because of its hydrophobic microdomains. The critical aggregation concentration (CAC), which was defined as the threshold concentration of self-assembly formation by intra- or intermolecular association, can be determined from the variation of the I_{372}/I_{385} value of pyrene in the presence of polymeric amphiphiles. Fig. 5(a) shows the variation of the I_{372}/I_{385} ratio of pyrene with the same concentration of CHC–PAA hybrid with various CHC : AA ratios, ranging from 1/1, 1/3 to 1/6. The CAC values for the CHCA1, CHCA3, and CHCA6 hybrids are determined to be 0.287 mg ml^{-1}, 0.348 mg ml^{-1} (check Fig. 5, it shows 0.35 mg ml^{-1}, but it seems to be the same from Fig. 5(b)), and 0.345 mg

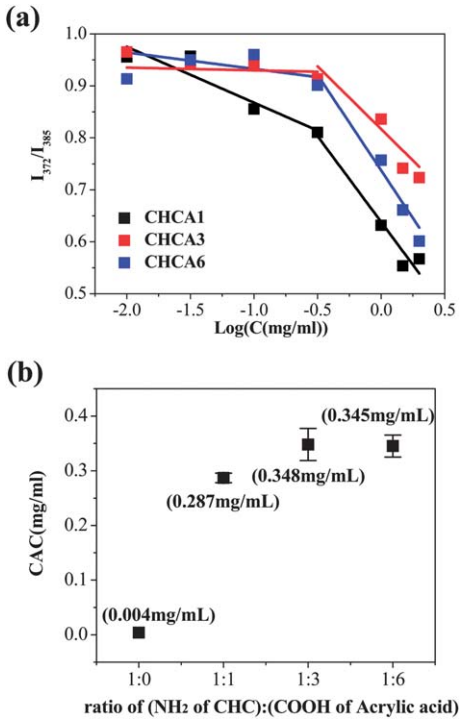

Fig. 5 (a) The value of I_{372}/I_{385} of pyrene with the concentration of CHC–PAA hybrids with various ratios of CHC : PAA. The intersection of the straight lines indicates the threshold of CAC, of the hybrids, which gives the value of (b) critical aggregation concentration (CAC) of pure CHC and CHC–PAA hybrids with different ratios of CHC : PAA.

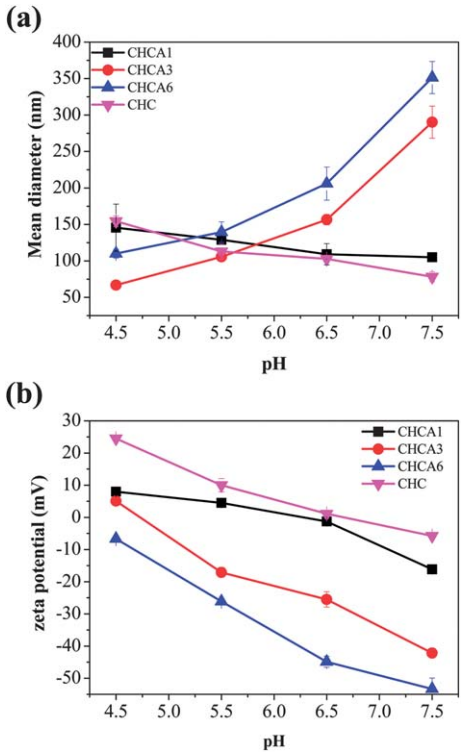

Fig. 6 The variation of (a) mean diameter and (b) zeta potential of CHC–PAA hybrid nanoparticles at different pH buffers. The final concentration of CHC–PAA in each sample is 0.1 mg ml^{-1} ($n = 3$).

ml^{-1}, respectively, as illustrated in Fig. 5(b). It pointed out that the CAC values increased with starting AA concentration, suggesting a decreased self-assembling capability as a result of the polymerization of more AA, *i.e.*, CHCA3 and CHCA6 compositions, due to the presence of branched PAA along the CHC backbone. The branched PAA may also account for the larger size of the resulting CHC–PAA nanoparticles to be discussed in forthcoming analysis. Further increase in AA did not alter CAC of the resulting hybrids, suggesting a balance between hydrophilic and hydrophobic contributions of the resulting CHC–PAA hybrids over the concentration range of AA in this study. The morphological structure of the resulting self-assembled CHC–PAA hybrids, as represented by CHCA3 composition, indicates a spherical nanostructure with relatively uniform size distribution, from TEM examination, as given in Fig. S1.†

3.4 pH-responsive mean size and zeta potential of CHC–PAA nanoparticles

The mean size of the CHC–PAA nanoparticles was measured by dynamic light scattering (DLS) as shown in Fig. 6(a), in terms of pH, ranging from 4.5 to 7.5. For pure CHC and small AA grafted samples, *i.e.*, CHCA1, particle size showed a linear decrease with increasing pH, suggesting that the nanostructure became more compact due to increased unprotonated amine groups with increasing pH. However, a significant increase in particle size with increasing pH was detected for the CHCA3 and CHCA6 compositions, having much more –COOH groups. The deprotonated hydroxyl groups increased significantly with increasing pH toward a basic environment, *i.e.*, at pH = 7.5, and this became more pronounced for CHCA6 composition, exhibiting the largest particle size among all. However, compared with the pH-dependent behavior among the CHC–PAA hybrids, CHCA3 demonstrated the greatest pH responsiveness to an extent as large as about 120 times, from pH 4.5 to pH 7.5. This pH-dependent volumetric change for the CHC–PAA hybrids with a CHC/AA = 1/3 composition was found to be the greatest among those similar materials reported in the literature by a factor of 10–100 times. For both CHCA3 and CHCA6 compositions having a much lower amine group and higher carboxylic group content, an increasing diameter of the CHC–PAA nanoparticles was detected with increased environmental pH. This observation indicates an increased degree of dissociation of the carboxylic groups from both PAA and CHC to form COO^- groups with increasing pH. An enhanced repulsive force over the dissociated PAA and CHC segments gave rise to an increase in swelling of the resulting CHC–PAA hybrids, thus, an increased size of the nanoparticles with increasing environmental pH.

As expected, the incorporation of AA into the CHC also causes a pronounced pH-dependent surface charge as shown in Fig. 6(b). The zeta potential of the hybrids turns to be more negative with AA and a more pH dependency was observed with increasing AA incorporation, which is in good agreement with the argument aforementioned. Such a higher pH dependency of the surface charge is also reflected in a more responsive volumetric change depicted in Fig. 6(a).

3.5 Drug loading and release from the hybrid nanoparticles

The hydrophobic drug (*S*)-(+)-camptothecin (CPT) was employed as a model molecule to further explore the potential uses of the hybrid for controlled drug delivery. In this evaluation, CHC and CHC–PAA powders were dissolved in 50 μg ml^{-1} CPT solution (DMSO/water (0.5/9.5 v/v ratio)) with different pH values from 4.5 to 7.5, separately. Table 3 shows that the CHC–PAA hybrids demonstrate much higher encapsulation efficiency, *i.e.*, 90–95%, with increasing AA, under various pH values than pure CHC, *i.e.*, 70–72%. The hybrid with more AA incorporation appears to accommodate more CPT upon self-assembly, thus, resulting in a higher encapsulation efficiency. PAA on the CHC–PAA nanoparticle trapped more CPT from the drug solution, and this influence was more conspicuous as the PAA amount increased. Besides, DMSO-assisted CPT dissolution suggested an improved hydrophilic affinity between the CHC–PAA hybrids and DMSO-associated CPT complexes, giving rise to a higher encapsulation efficiency upon self-assembly. However, for a given hybrid composition, the encapsulation efficiency appeared to be independent of the solution pH, suggesting that both the size and degree of ionization (particle charging) of a given hybrid composition exerted a negligible influence on drug encapsulation.

The release profiles of CHC–PAA nanoparticles at pH 4.5 and 7.5 are compared as shown in Fig. 7 and the associated release kinetic analysis is given in Table S1.† A burst-like CPT release is observed for pure CHC nanoparticles, but becomes much slower for the CHC–PAA hybrids at pH 4.5, Fig. 7(a). However, under near physiological conditions, *i.e.*, pH 7.5, the release rate of CHC–PAA hybrid nanoparticles becomes faster than that of pure CHC (Fig. 7(b)). It is reasonable to realize that at acidic pH, protonation of amine groups of CHC caused swelling, leading to a higher release rate. However, the swelling due to the presence of the smaller amount of amine groups of CHC–PAA hybrids became less pronounced, resulting in a slower release profile. In contrast, a greater amount of carboxyl groups of CHC–PAA hybrids were subjected to ionization at pH 7.5, giving rise to extensive volumetric dilation (swelling), especially for CHCA3 composition, accompanied by an enhanced release kinetic. This result is in good agreement with the effect of the pH on the variation of size or volume of the hybrid nanoparticle abovementioned. Furthermore, these experimental observations suggest a potential application of the CHC–PAA hybrid nanoparticles as oral drug delivery vehicles.

Table 3 Drug encapsulated efficiency (EE) of CHC–PAA hybrid nanoparticles under various pH values ($n = 3$)

Sample	EE @ pH 4.5 (%)	EE @ pH 6.5 (%)	EE @ pH 7.5 (%)
CHC	69.8 ± 0.8	72 ± 0.5	72.1 ± 1.1
CHCA1	89.3 ± 1.3	90.6 ± 1.1	91 ± 2.8
CHCA3	94.3 ± 2.1	94.2 ± 1.3	94.3 ± 0.5
CHCA6	94.8 ± 0.5	94.8 ± 1.2	94.6 ± 1

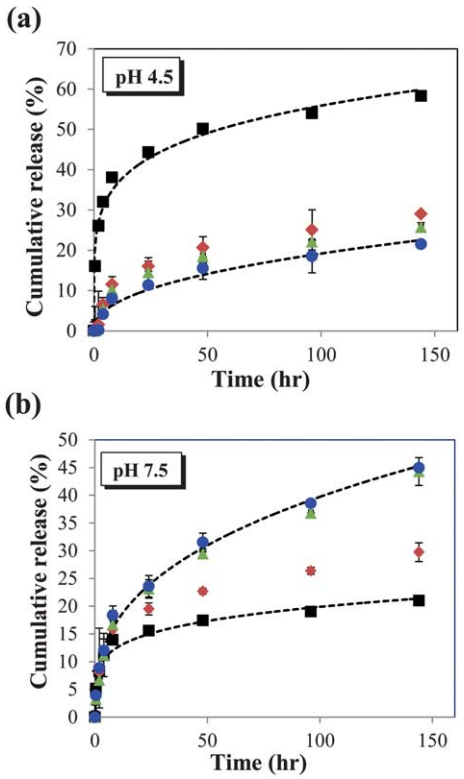

Fig. 7 *In vitro* release profiles of CPT from CHC–PAA nanoparticles at (a) pH 4.5 and (b) pH 7.5 medium at 25 °C; CHC (■), CHCA1 (◆), CHCA3 (▲) and CHCA6 (●). Error bars indicate standard deviation ($n = 3$).

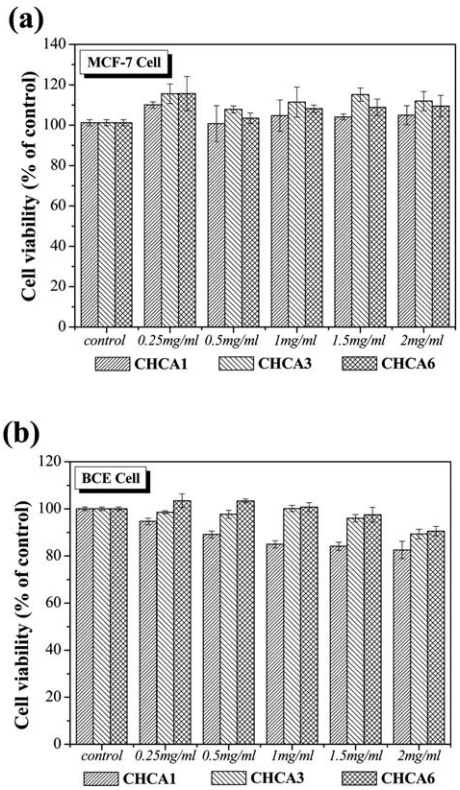

Fig. 8 The cell viability of (a) MCF-7 and (b) BCE cells incubated with different concentrations of CHC–PAA hybrid nanoparticles for 24 hours ($n = 3$).

3.6 Cytotoxic assay

The cytotoxicity of different CHC–PAA (CHCA1, CHCA3 and CHCA6) hybrids against the human breast adenocarcinoma cell line (MCF-7) is shown in Fig. 8(a). The MCF-7 cells were treated with different concentrations (2, 1.5, 1, 0.5 and 0.25 mg ml^{-1}) of CHC–PAA nanoparticles, after 24 hours of incubation, the cell viability of CHC–PAA ranged from 100–115%, indicating excellent cytocompatibility of the hybrids toward the human breast adenocarcinoma cell.

Using the MTT assay, the cytotoxicity of CHC–PAA nanoparticles against bovine cornea endothelial (BCE) cells was evaluated and is illustrated in Fig. 8(b). After 24 hours of incubation, the CHC–PAA nanoparticles with relatively high doses ranging from 0.25, 0.5, 1.0, 1.5 to 2 mg ml^{-1} showed reasonably good compatibility with cell viability remaining above 90% for CHCA3 and CHCA6 compositions, and was slightly above 80% for the CHCA1 hybrid. In short, this preliminary viability test confirmed the CHC–PAA hybrids to be a new class of biomaterials and can be potentially adaptable for a wide range of biomedical applications such as oral drug delivery.

4 Conclusion

CHC–PAA hybrids were successfully prepared by free radical polymerization of acrylic acid (AA) monomers in the presence of an amphiphilic carboxymethyl-hexanoyl chitosan (CHC). These CHC–PAA hybrids were designed to have a much higher pH-responsive behavior in terms of size or volume than existing reports in the literature and are aimed to use for drug delivery applications. Structural characterizations confirmed substantial amounts of AA were successfully grafted onto amine groups in the CHC *via* radical reactions, while the hydrophobic segments remained intact. Such AA substitution gives rise to a much higher pH responsiveness in terms of size and the largest volumetric change, by as much as 120 times, was detected between pH 4.5 and pH 7.5, covering a range of pH between normal and cancerous cells. Such a pH-responsive behavior renders a robust control of drug release shifting between acidic and basic environments and can be a potential candidate for oral drug delivery applications. Moreover, the CHC–PAA hybrids also demonstrated efficient cellular internalization and outstanding cytocompatibility toward both cancerous cells (MCF-7) and normal cells (BCE), implying a new class of biomaterial for cellular-based therapeutics.

Acknowledgements

The authors would like to thank the National Science Council, Taiwan, Republic of China, for the financial support under a project contract of NSC-100-2622-M-009-002-CC3.

References

1 N. Nasongkla, X. Shuai, H. Ai, B. D. Weinberg, J. Pink, D. A. Boothman and J. Gao, *Angew. Chem.*, 2004, **116**, 6483–6487.
2 C. Oerlemans, W. Bult, M. Bos, G. Storm, J. F. Nijsen and W. Hennink, *Pharm. Res.*, 2010, **27**, 2569–2589.
3 W. Wang, D. Cheng, F. Gong, X. Miao and X. Shuai, *Adv. Mater.*, 2012, **24**, 115–120.
4 M. Stubbs, P. M. J. McSheehy, J. R. Griffiths and C. L. Bashford, *Mol. Med. Today*, 2000, **6**, 15–19.
5 E. S. Lee, K. Na and Y. H. Bae, *J. Controlled Release*, 2003, **91**, 103–113.
6 Y. Bae, S. Fukushima, A. Harada and K. Kataoka, *Angew. Chem., Int. Ed.*, 2003, **42**, 4640–4643.
7 Y. Bae, N. Nishiyama, S. Fukushima, H. Koyama, M. Yasuhiro and K. Kataoka, *Bioconjugate Chem.*, 2004, **16**, 122–130.
8 K. Kataoka, A. Harada and Y. Nagasaki, *Adv. Drug Delivery Rev.*, 2001, **47**, 113–131.
9 H. S. Yoo and T. G. Park, *J. Controlled Release*, 2001, **70**, 63–70.
10 S. J. Lee, H. Koo, H. Jeong, M. S. Huh, Y. Choi, S. Y. Jeong, Y. Byun, K. Choi, K. Kim and I. C. Kwon, *J. Controlled Release*, 2011, **152**, 21–29.
11 N. Nishiyama and K. Kataoka, *Pharmacol. Ther.*, 2006, **112**, 630–648.
12 T. Nakanishi, S. Fukushima, K. Okamoto, M. Suzuki, Y. Matsumura, M. Yokoyama, T. Okano, Y. Sakurai and K. Kataoka, *J. Controlled Release*, 2001, **74**, 295–302.
13 H. Zhu, F. Liu, J. Guo, J. Xue, Z. Qian and Y. Gu, *Carbohydr. Polym.*, 2011, **86**, 1118–1129.
14 J. Hyung Park, S. Kwon, M. Lee, H. Chung, J.-H. Kim, Y.-S. Kim, R.-W. Park, I.-S. Kim, S. Bong Seo, I. C. Kwon and S. Young Jeong, *Biomaterials*, 2006, **27**, 119–126.
15 H. Zhou, W. Yu, X. Guo, X. Liu, N. Li, Y. Zhang and X. Ma, *Biomacromolecules*, 2010, **11**, 3480–3486.
16 G. Saravanakumar, K. H. Min, D. S. Min, A. Y. Kim, C.-M. Lee, Y. W. Cho, S. C. Lee, K. Kim, S. Y. Jeong, K. Park, J. H. Park and I. C. Kwon, *J. Controlled Release*, 2009, **140**, 210–217.
17 H. Zheng, Y. Rao, Y. Yin, X. Xiong, P. Xu and B. Lu, *Carbohydr. Polym.*, 2011, **83**, 1952–1958.
18 S. Y. Chae, S. Son, M. Lee, M.-K. Jang and J.-W. Nah, *J. Controlled Release*, 2005, **109**, 330–344.
19 K. Kim, J. H. Kim, H. Park, Y.-S. Kim, K. Park, H. Nam, S. Lee, J. H. Park, R.-W. Park, I.-S. Kim, K. Choi, S. Y. Kim, K. Park and I. C. Kwon, *J. Controlled Release*, 2010, **146**, 219–227.
20 J. J. Wang, Z. W. Zeng, R. Z. Xiao, T. Xie, G. L. Zhou, X. R. Zhan and S. L. Wang, *Int. J. Nanomed.*, 2011, **6**, 765–774.
21 Z. Liu, Y. Jiao, Y. Wang, C. Zhou and Z. Zhang, *Adv. Drug Delivery Rev.*, 2008, **60**, 1650–1662.
22 C.-M. Lee, D. Jang, J. Kim, S.-J. Cheong, E.-M. Kim, M.-H. Jeong, S.-H. Kim, D. W. Kim, S. T. Lim, M.-H. Sohn, Y. Y. Jeong and H.-J. Jeong, *Bioconjugate Chem.*, 2011, **22**, 186–192.
23 S. Zhang, Y. Li, G. Ren, X. Chen and X. Meng, *J. Appl. Polym. Sci.*, 2011, **121**, 3359–3367.
24 C. Zheng, J. Xu, X. Yao, J. Xu and L. Qiu, *J. Colloid Interface Sci.*, 2011, **355**, 374–382.
25 F.-Q. Hu, L.-N. Liu, Y.-Z. Du and H. Yuan, *Biomaterials*, 2009, **30**, 6955–6963.

26 J. S. Park, T. H. Han, K. Y. Lee, S. S. Han, J. J. Hwang, D. H. Moon, S. Y. Kim and Y. W. Cho, *J. Controlled Release*, 2006, **115**, 37–45.
27 Y. Jin, H. Hu, M. Qiao, J. Zhu, J. Qi, C. Hu, Q. Zhang and D. Chen, *Colloids Surf., B*, 2012, **94**, 184–191.
28 C. Y. Chuang, T. M. Don and W. Y. Chiu, *J. Polym. Sci., Part A: Polym. Chem.*, 2009, **47**, 2798–2810.
29 M. D. Kurkuri and T. M. Aminabhavi, *J. Controlled Release*, 2004, **96**, 9–20.
30 W. T. Wu, M. Aiello, T. Zhou, A. Berliner, P. Banerjee and S. Q. Zhou, *Biomaterials*, 2010, **31**, 3023–3031.
31 K. H. Liu, S. Y. Chen, D. M. Liu and T. Y. Liu, *Macromolecules*, 2008, **41**, 6511–6516.
32 T. Y. Liu, S. Y. Chen, Y. L. Lin and D. M. Liu, *Langmuir*, 2006, **22**, 9740–9745.
33 T.-Y. Liu, S.-Y. Chen, Y.-L. Lin and D.-M. Liu, *Langmuir*, 2006, **22**, 9740–9745.
34 M. Friedman, *J. Agric. Food Chem.*, 2004, **52**, 385–406.
35 E. Curotto and F. Aros, *Anal. Biochem.*, 1993, **211**, 240–241.
36 Y. Hu, X. Jiang, Y. Ding, H. Ge, Y. Yuan and C. Yang, *Biomaterials*, 2002, **23**, 3193–3201.
37 C.-L. Lin, C.-F. Lee and W.-Y. Chiu, *J. Colloid Interface Sci.*, 2005, **291**, 411–420.
38 N. Barbani, L. Lazzeri, C. Cristallini, M. G. Cascone, G. Polacco and G. Pizzirani, *J. Appl. Polym. Sci.*, 1999, **72**, 971–976.
39 J. Liu, W. Wang and A. Wang, *Polym. Adv. Technol.*, 2011, **22**, 627–634.
40 L. S. Fu, R. A. S. Ferreira, N. J. O. Silva, L. D. Carlos, V. D. Bermudez and J. Rocha, *Chem. Mater.*, 2004, **16**, 1507–1516.

